



HAL
open science

Building a boiling-flow multiphase CFD framework for interfacial area and heat transfer modeling

Corentin Reiss, Antoine Gerschenfeld, Catherine Colin

► **To cite this version:**

Corentin Reiss, Antoine Gerschenfeld, Catherine Colin. Building a boiling-flow multiphase CFD framework for interfacial area and heat transfer modeling. NURETH20 - 20th International Topical Meeting on Nuclear Reactor Thermal Hydraulics, Aug 2023, Washington, United States. pp.225-238. cea-04190863

HAL Id: cea-04190863

<https://cea.hal.science/cea-04190863v1>

Submitted on 30 Aug 2023

HAL is a multi-disciplinary open access archive for the deposit and dissemination of scientific research documents, whether they are published or not. The documents may come from teaching and research institutions in France or abroad, or from public or private research centers.

L'archive ouverte pluridisciplinaire **HAL**, est destinée au dépôt et à la diffusion de documents scientifiques de niveau recherche, publiés ou non, émanant des établissements d'enseignement et de recherche français ou étrangers, des laboratoires publics ou privés.

Building a Boiling-Flow Multiphase CFD Framework for Nuclear Reactor Conditions

Corentin Reiss and Antoine Gerschenfeld

Université Paris-Saclay, CEA,
Service de Thermo-hydraulique et de Mécanique des Fluides, 91191, Gif-sur-Yvette, France.
corentin.reiss@cea.fr; antoine.gerschenfeld@cea.fr

Catherine Colin

Institut de Mécanique des Fluides de Toulouse, Université de Toulouse, CNRS, INPT, UPS,
Allée du Prof. Camille Soula, 31400 Toulouse, France
catherine.colin@toulouse-inp.fr

ABSTRACT

Multiphase CFD's predictions for boiling flow are limited by available models for interfacial heat transfer and area [1]. Both terms are greatly interdependent. Much research has relied upon adiabatic experiments on bubbly flow to determine the contribution of coalescence and breakup terms on the interfacial area independently of heat transfer. These models are often applied to boiling flows [2].

We develop a two-fluid Euler-Euler CFD framework based on the PolyMAC numerical scheme [3] in CEA's open-source TrioCFD code [4]. We implement a $k - \omega$ [5] turbulence model, along with an original adaptive wall law treatment. Interfacial momentum closure terms are selected and validated using bubbly adiabatic experiments on vertical flows [6]. The local experimental bubble diameter is enforced to limit interactions with interfacial area closures, as in [7].

We simulate the Debora experiment [8], an ascending boiling freon flow in a tube, and again use the experimental diameter. The long-term goal is to run simulations using independently selected coalescence-fragmentation and heat transfer closures.

KEYWORDS

Multiphase CFD, Interfacial forces, Interfacial heat flux

1. INTRODUCTION

Understanding multiphase flows is critical for nuclear applications [9, 10]. However, these flows are extremely complex and a wide variety of flow patterns can exist [11]. Even restricting ourselves to bubbly flows, all configurations cannot be reliably simulated using existing Computational Fluid Dynamics (CFD) codes [1]. Predicting the void fraction distribution in a boiling nuclear sub-channel requires a knowledge of liquid turbulence, interfacial forces, wall boiling dynamics, condensation and bubble coalescence and fragmentation. Additionally, these terms interact with each other. For example, coalescence will affect bubble diameters, which will change their velocities and condensation rates, and the global mass, momentum and energy balances. This makes it very difficult to separate contributions and makes error compensation possible [12]. Therefore, the models commonly used are mostly derived from simple situations very different from reactors, like the study of adiabatic single bubbles at atmospheric pressure [13].

In this paper, we contribute to building a CFD framework to study Pressurized Water Reactor (PWR) conditions. Our approach consists in exploiting existing experiments in such a way as to decouple the contributions of aforementioned terms. To avoid uncertainty related to interfacial area transport equations [14] or population balance [15, 16] methodologies, we use bubbly flows with measured mean Sauter diameters and enforce the experimental values as in [17]. We implement standard single phase turbulence and bubbly flow closure terms [2, 7, 18] and validate them on air-water bubbly flows in pipes at atmospheric pressure [6, 19] (see figure 1).

We then study the Debora experiment [8] (see figure 1). This is a vertical heated tube filled with flowing Freon-12 designed to fill similarity criteria with PWR and Boiling Water Reactor conditions. Void fraction, mean Sauter diameter and temperature measures were taken for different pressures, flow rates, heat fluxes and inlet subcoolings. We run simulations using the standard closure terms calibrated at atmospheric pressures, which yield unsatisfying results. We then evaluate the sensitivity of the simulation results to these closures by modifying some of them.

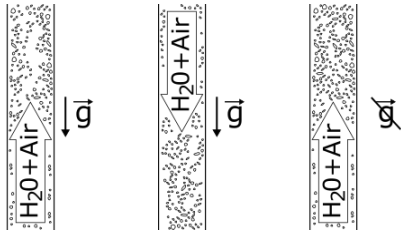
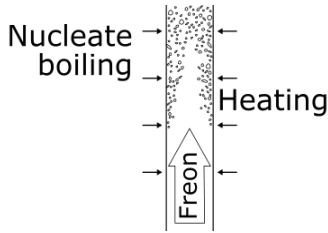
Experiment	Measured quantities	Models validated
<p>Hibiki et al. [19], Colin et al. [6]</p> 	<p>Gas & Liquid velocity Gas & Liquid vel. fluct. Void fraction, Sauter diam.</p>	<p>Lift force Turbulent disp. force Wall repulsion force</p>
<p>DEBORA [8]</p> 	<p>Gas velocity & vel. fluct. Liquid temperature Void fraction, Sauter diam.</p>	<p>Wall heat flux partition Interfacial heat transfer</p>

Figure 1. Diagrams of the two-phase experiments used for framework validation and heat transfer models evaluation.

2. PHYSICAL MODEL

2.1. TrioCFD and PolyMAC

CEA is developing a multiphase RANS CFD module in its open-source CFD code, TrioCFD [4]. This module, called TrioCMFD (Computational Multiphase Fluid Dynamics), is based on the PolyMAC Finite Volume numerical scheme developed by Gerschenfeld and Gorse for component-scale codes [3]. PolyMAC can handle mass, momentum and energy conservation equations for an arbitrary number of fluids in an Euler-Euler framework [11]. The semi-conservative form of the momentum equation is used [20]. The equations that govern a phase k are:

$$\begin{aligned}
\frac{\partial \alpha_k \rho_k}{\partial t} + \nabla \cdot (\alpha_k \rho_k \vec{u}_k) &= \Gamma_k \\
\alpha_k \rho_k \frac{\partial \vec{u}_k}{\partial t} + \nabla \cdot (\alpha_k \rho_k \vec{u}_k \otimes \vec{u}_k) - \vec{u}_k \nabla \cdot (\alpha_k \rho_k \vec{u}_k) &= \\
-\alpha_k \nabla P + \nabla \cdot [\alpha_k \mu_k \nabla \vec{u}_k - \alpha_k \rho_k \overline{u'_i u'_j}] + \vec{F}_{ki} + \alpha_k \rho_k \vec{g} &= \quad (1) \\
\frac{\partial \alpha_k \rho_k e_k}{\partial t} + \nabla \cdot (\alpha_k \rho_k e_k \vec{u}_k) &= \\
-P (\partial_t \alpha_k + \nabla \cdot (\alpha_k \vec{u}_k)) + \nabla \cdot [\alpha_k \lambda_k \nabla T_k - \alpha_k \rho_k \overline{u'_i e'_k}] + q_{ki} + q_{kw} &=
\end{aligned}$$

In equation 1, the terms that need closure laws are the turbulent terms $\overline{u'_i u'_j}$ and $\overline{u'_i e'_k}$, the mass transfer term Γ_k , the interfacial force term \vec{F}_{ki} , the interfacial heat transfer q_{ki} and the wall heat transfer q_{kw} .

In this paper, we work with two fluids: a liquid phase l and a gas phase g .

2.2. Turbulence modelling

Shear-Induced Turbulence We choose to use a two-equations turbulence model as for single-phase flows in rod bundles, it yields similar results as RSM models with faster calculation times [21]. We select the Kok $k-\omega$ turbulence model [5] as it has similar properties to the more commonly used Menter $k-\omega$ model [22], i.e., a cross-diffusion term that is suppressed in the near-wall region, but is easier to implement. To adapt this model to two-phase flows, we chose to write an equation on $\alpha_l \rho_l k$ and not merely on k as the turbulent kinetic energy is in the liquid phase and is a conserved quantity. ω being a frequency, we write the turbulent equation directly on it. This yields:

$$\begin{aligned}
\nu_t &= \frac{k}{\omega} & \overline{u'_i u'_j} &= -\nu_t \nabla \vec{u}_l & \overline{u'_i e'_l} &= -\nu_t C_{p,l} \nabla T_l \\
\partial_t (\alpha_l \rho_l k) + \nabla \cdot (\alpha_l \rho_l k \vec{u}_l) &= \alpha_l \rho_l \nu_t (\nabla \vec{u}_l + {}^t \nabla \vec{u}_l) \cdot \nabla \vec{u}_l - \beta_k \alpha_l \rho_l k \omega + \nabla \cdot (\alpha_l \rho_l (\nu_l + \sigma_k \nu_t) \nabla k) \\
\partial_t \omega + \nabla \cdot (\alpha_l \omega \vec{u}_l) &= \alpha_\omega \frac{\omega}{k} \nu_t (\nabla \vec{u}_l + {}^t \nabla \vec{u}_l) \cdot \nabla \vec{u}_l - \beta_\omega \omega^2 + \nabla \cdot ((\nu_l + \sigma_\omega \nu_t) \nabla \omega) \\
&+ \sigma_d \frac{1}{\omega} \max \{ \nabla k \cdot \nabla \omega, 0 \}
\end{aligned} \quad (2)$$

The values of the constants are $\alpha_\omega = 0.5$, $\beta_k = 0.09$, $\beta_\omega = 0.075$, $\sigma_k = 2/3$, $\sigma_\omega = 0.5$ and $\sigma_d = 0.5$.

We implement an adaptive wall-law algorithm that begins by determining the friction velocity u_τ in the same way as in the Fun3D code [23]. The shear stress at the boundary is then computed and is used as a Navier boundary condition for the momentum equation: $\tau_{wf} = \alpha_l \rho_l u_\tau^2$.

The boundary condition on k is $k = 0$ at the wall for $y_+ < 10$, where $y_+ = y u_\tau / \nu_l$ and y is the distance between the wall and the first element center. For larger wall elements, it is a zero-flux condition. The transition is smoothed by a transition factor $\tanh((y_+/10)^2)$.

For ω , Knopp et al. [24] give an analytical value in the near-wall region. A simple solution would be to enforce this value in the first element. However, was already used in TrioCFD and creates numerical issues for tetrahedron meshes. Instead, we calculate the analytical solution at a distance $y/2$ from the wall. We then enforce a Dirichlet boundary condition at the wall for the first element: $\omega_{\text{wall}} = 2 \cdot \omega(y/2)$. This amounts to creating a virtual element between the first element and the wall in which we know the value of ω .

The single-phase heat transfer coefficient that we have implemented is the one proposed by Kader [25]. He gives an expression of $\theta_+(Pr, y_+)$, where $\theta_+ = (T_w - T_l)/T_*$, $T_* = \Phi/(\rho_l C_p u_\tau)$ and Φ is the wall heat flux. It is based on experimental measures for y_+ ranging from 0 to 300. Using the previously calculated expression of u_τ , we calculate θ_+ and a wall heat transfer coefficient. We use the Kader expression as the convective heat transfer contribution in our wall heat flux partition model (see section 2.4).

Bubble-Induced turbulence According to Alm eras et al., liquid velocity fluctuations induced by bubble movements are small before those from shear if the bubbance parameter $b = \frac{\alpha_g \|\vec{u}_g - \vec{u}_l\|^2}{u_{1\phi}^2} < 0.5$ [26]. At PWR pressures, $d_b < 1\text{mm}$, which yields $\|\vec{u}_g - \vec{u}_l\| < 0.1\text{m/s}$, and $\alpha_g < 0.5$. Using the Reichardt correlation [27] for $Re = 10^5$, bubble-induced turbulence can be neglected in PWR's (i.e. $b < 0.5$) for $u_{\text{bulk}} > 1.5\text{m/s}$. This is a low value as $u_{\text{bulk}} \sim 4\text{m/s}$ in operation [9], and $b \sim 0.1$. Therefore, we do not model bubble-induced turbulence.

2.3. Interfacial Force Term Modeling

The interfacial force exerted by the liquid on the gas is $\vec{F}_{gi} = -\vec{F}_{li}$. In this subsection, all forces written apply to the gas phase. We separate the interfacial force term in five different contributions:

$$\vec{F}_{gi} = \vec{F}_{\text{drag}} + \vec{F}_{\text{VM}} + \vec{F}_{\text{lift}} + \vec{F}_{\text{TD}} + \vec{F}_{\text{wall}} \quad (3)$$

Drag Force We implement the contaminated drag force of Tomiyama et al. [28]:

$$\vec{F}_{\text{drag}} = -\frac{3}{4}C_D \frac{\alpha_g \rho_l}{d_b} \|\vec{u}_g - \vec{u}_l\| (\vec{u}_g - \vec{u}_l) \quad , \quad C_D = \max\left(\frac{24}{Re_b}(1 + .15Re^{.687}), \frac{8Eo}{3Eo + 12}\right) \quad (4)$$

Virtual Mass Force The virtual mass writes:

$$\vec{F}_{\text{VM}} = -C_{VM} (\partial_t \vec{u}_g - \partial_t \vec{u}_l + \vec{u}_g \nabla \vec{u}_g - \vec{u}_l \nabla \vec{u}_l) \quad (5)$$

The most commonly used formulations are the constant coefficient $C_{VM} = \frac{1}{2}\alpha_g$ [29] and the Zuber coefficient $C_{VM} = \frac{1}{2} \frac{1+2\alpha_g}{1-\alpha_g} \alpha_g$ [30], that were both derived theoretically. Recently, Beguin et al. [31] performed potential flow simulations with random bubble positions and found $C_{VM} = \alpha_g (\frac{1}{2} + 0.34\alpha_g^2) \sim \frac{1}{2}\alpha_g$. Furthermore, in some Debora experimental runs [32], the local void fraction can reach 0.7. In either above formulation, a liquid fraction of at least $0.7 \cdot 1/2 = 0.35$ would be entrained even though the total liquid fraction is 0.3. This is non-physical and leads to numerical stability issues. We therefore assume that at most 1/2 of the remaining liquid can be entrained by the gas, the value 1/2 being arbitrary. This leads to:

$$C_{VM} = \min\left(\frac{1}{2}\alpha_g, \frac{1}{2}\alpha_l\right) \quad (6)$$

Our modification affects C_{VM} for $\alpha_g > 0.5$.

Lift Force The general formulation for the lift force is:

$$\vec{F}_{\text{lift}} = -C_L \rho_l \alpha_g (\vec{u}_g - \vec{u}_l) \wedge (\nabla \wedge \vec{u}_l) \quad (7)$$

The difference between lift force models is the lift coefficient C_L . A constant coefficient can be chosen by the user. The Sugrue et al. [17] formulation was also implemented, as it was designed to operate on high-void fraction ascending flows and not only single bubbles, contrarily to the Tomiyama et al. formulation [13]. It reads:

$$C_L = f(Wo) \cdot g(\alpha) \quad Wo = Eo \frac{k}{\|\vec{u}_g - \vec{u}_l\|^2} \quad (8)$$

$$f(Wo) = \min(0.03, 5.0404 - 5.0781Wo^{0.0108}) \quad g(\alpha) = 1.0155 - 0.0154\exp(8.0506\alpha)$$

Turbulent Dispersion Force We select the Burns et al. force [33]:

$$\vec{F}_{\text{disp}} = -C_{TD} \rho_l k \nabla \alpha_g, \quad C_{TD} = \frac{3}{4} \frac{C_D}{d_b} |\vec{u}_g - \vec{u}_l| \frac{1}{0.9 \cdot \omega} \left(1 + \frac{\alpha_g}{\alpha_l}\right) \quad (9)$$

Wall Correction The main wall correction term implemented is the one proposed by Lubchenko et al. [34]. It is based on geometrical arguments. It suppresses lift and modifies turbulent dispersion close to the wall. The lift coefficient becomes:

$$C_L \rightarrow \begin{cases} 0 & \text{if } y/d_b < 1/2 \\ C_L \left(3 \left(\frac{2y}{d_b} - 1\right)^2 - 2 \left(\frac{2y}{d_b} - 1\right)^3\right) & \text{if } 1/2 \leq y/d_b < 1 \\ C_L & \text{if } y/d_b \geq 1 \end{cases} \quad (10)$$

If \vec{n} is the unit vector normal to the wall, the turbulent dispersion wall correction writes:

$$\vec{F}_{\text{wall}} = \begin{cases} C_{TD} \rho_l k \cdot \alpha_g \frac{1}{y} \frac{d_B - 2y}{d_B - y} \vec{n} & \text{if } y/d_b < 1/2 \\ 0 & \text{if } y/d_b \geq 1/2 \end{cases} \quad (11)$$

2.4. Heat and Mass transfers

Interfacial heat transfer As we study bubbly flows, we select Nusselt-based interfacial heat transfer formulations:

$$q_{ki} = \frac{6\alpha_g}{d_b} \frac{\lambda_l}{d_b} (T_g - T_l) Nu \quad (12)$$

The Ranz-Marshall ($Nu = 2 + 0.6Re_b^{1/2} Pr^{1/3}$) [35] and the Zeitoun et al. ($Nu = 2.04Re_b^{0.61} \alpha_g^{0.328} Ja^{-0.308}$) [36] models are implemented.

Wall heat transfer The Kurul-Podowski [37] model was selected.

$$\Phi_{KP} = \Phi_c + \Phi_q + \Phi_e \quad (13)$$

Where Φ_c is the convective heat flux, Φ_q the quenching heat flux and Φ_e the evaporation heat flux. The detachment bubble diameter is $d_{b, \text{det}} = 10^{-4} \cdot (T_w - T_s) + 0.0014$, the nucleation site density $N_s = (210(T_w - T_s))^{1.8}$, the bubble fraction $A_b = \min(1, \pi/4 \cdot N_s d_{b, \text{det}}^2)$, the departure frequency $f_{\text{dep}} = \sqrt{\frac{4}{3} \frac{g(\rho_l - \rho_g)}{\rho_l d_{b, \text{det}}}}$. This yields:

$$\begin{aligned}\Phi_c &= (1 - A_b)\Phi_{1 \text{ phase}} \\ \Phi_e &= \frac{\pi}{6} f_{\text{dep}} d_{b, \text{det}}^3 \rho_g L_{\text{vap}} N_s \\ \Phi_q &= 2A_b \lambda_l (T_w - T_l) \sqrt{\frac{f_{\text{dep}} \rho_l C_{pl}}{\pi \lambda_l}}\end{aligned}\quad (14)$$

Where $\Phi_{1 \text{ phase}}$ comes from Kader [25].

3. FRAMEWORK VALIDATION

3.1. Adiabatic Single-Phase

We run simulations of flow in a same 2D channel at $Re = 20,000$ with cartesian grids of varying refinements: y_+ in the first element ranges from 3 to 229 (see figure 2). The results are independent of y_+ in the first element and consistent with literature and refined solutions, except for k_+ in the near-wall region which is expected as we are transitioning from a wall-resolved to a wall-modeled solution. We also simulate pipe flow experiments with various tube diameters and fluids, from Colin et al. [6] (see figure 3-A,B). The simulated velocity and velocity fluctuations match experimental results. This validates our implementation of single-phase turbulence and adaptive wall laws.

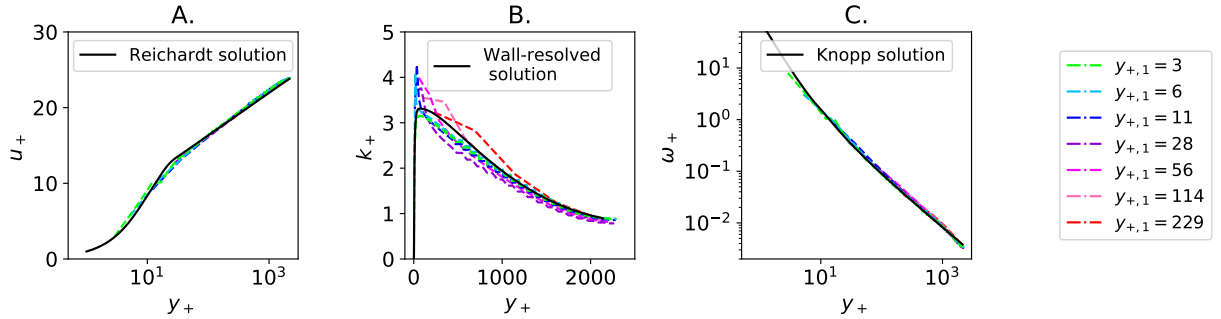


Figure 2. $k - \omega$ results for a turbulent 2D channel with $Re = 20,000$. The size of the first element at the wall, and therefore y_+ , varies in each simulation. **A.** Non-dimensional velocity $u_+ = u/u_\tau$ as a function of y_+ . Black line: Reichardt solution [27]. **B.** Non-dimensional turbulent kinetic energy $k_+ = k/u_\tau^2$ as a function of y_+ . Black line: refined solution for $y_{+,1} = 1$. **C.** Non-dimensional dissipation rate $\omega_+ = \omega u_\tau / \nu$ as a function of y_+ . Black line: Knopp solution [24].

3.2. Heated Single-Phase

One of the campaigns on the Debora experiment consisted in measuring the liquid R12 temperature for different flow rates, pressures and heating power [8]. We simulate single-phase heated flows from this campaign (see figure 3-C). The liquid temperature from the experiment and the simulation have the same profile shape, though they are off by $\sim 1^\circ\text{C}$. This amounts to a 5% power loss on the experimental setup. In our boiling Debora simulations, we reduce the power boundary condition by 5% to account for this.

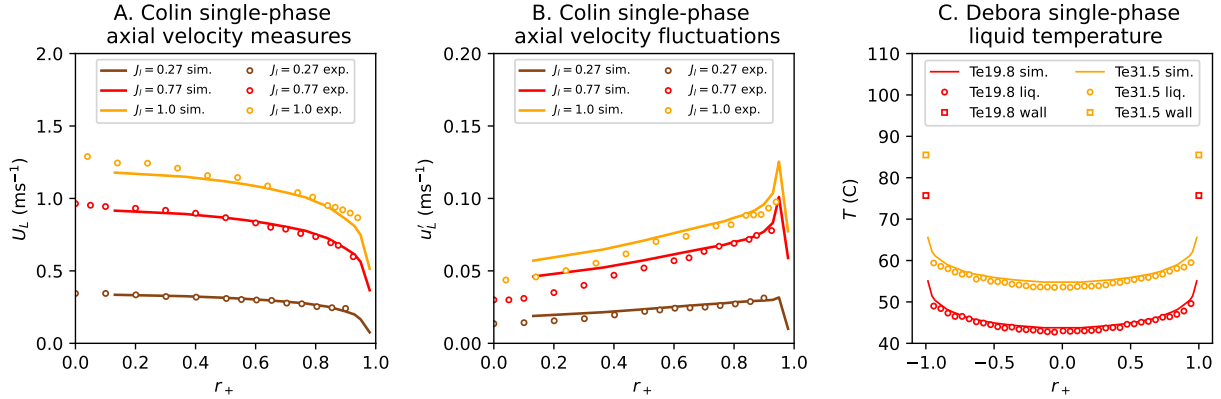


Figure 3. Single-phase validation of TrioCMFD. A. Colin et al. [6] single-phase axial velocity in a 4cm-diameter pipe. B. Colin et al. [6] single-phase axial velocity fluctuations in a 4cm-diameter pipe. C. Temperature profiles from single-phase Debora runs for a 19.2mm diameter pipe, 2.61MPa pressure, 1996kg/(m²s) mass velocity and 74.4kW/m² heat flux with inlet temperatures of 19.84°C and 31.46°C (page 109 in [8]).

3.3. Mesh Refinement

To evaluate the mesh sensitivity of TrioCMFD, we use test case U1 from [6]. Using SALOME [38], we mesh a disk with quadrilaterals and extrude it to obtain a hexahedral pipe mesh. We run simulations on a full cylinder, a quarter of a cylinder and an eighth of a cylinder with symmetry boundary conditions on vertical planes, and on a 2° slice only one element wide. Each mesh can have 7, 14 or 28 radial elements, and 40, 80 or 160 vertical elements. There is a significant difference between 7 and 14 radial element results, but virtually none between 14 and 28. Calculations that run on a cylinder or a slice give identical results, therefore to save computation time we only simulate slices in the rest of this paper.

3.4. Two-Phase Adiabatic Vertical Tube

Multiple experimental databases are available to study two-phase pipe flow. To validate TrioCMFD, we select the Hibiki et al. database for upwards flow [19], as it covers a broad range of liquid and gas injection fluxes. We also select the Colin et al. experiments for downwards and microgravity flow [6] (see figure 1). We run different test cases using the interfacial force models described in section 2.3 (see figure 4). To avoid modeling the interfacial area, we enforce the radially-dependent steady-state experimental diameter in the simulations. The complete model is able to predict correctly void fraction profiles for low (figure 4-A) and high (figure 4-C) liquid fluxes, in wall-peaked and core-peaked situations respectively. The prediction of the transition between both regimes can still be improved, as can be seen in figure 4-B. Furthermore, in figure 4-D the gas velocities are well predicted by the model.

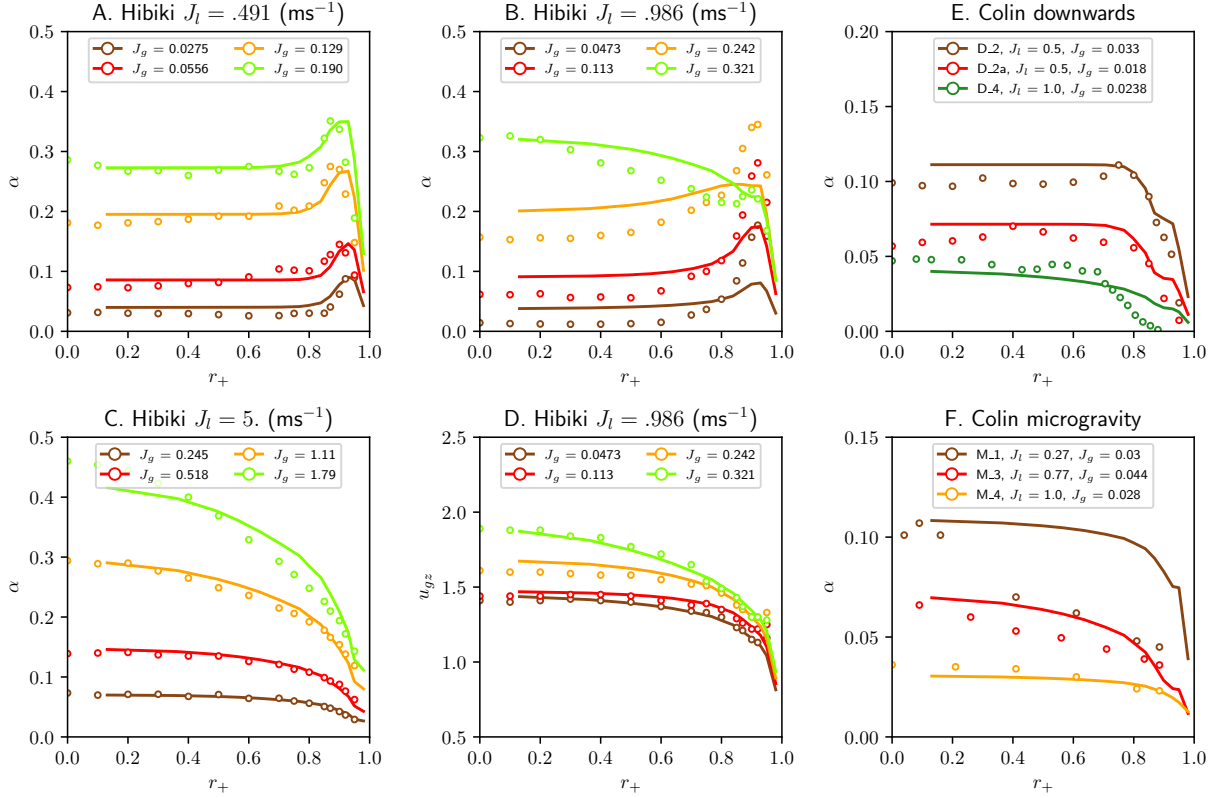


Figure 4. Two-phase adiabatic simulated and experimental void fraction distributions in a pipe. We use the interfacial force models described in section 2.3. Lines: simulations. Circles: experimental results. A-C. Void fraction results in Hibiki et al. [19] upwards flow experiments. D. Axial gas velocity results in Hibiki et al. [19] upwards flow experiments. E. Void fraction results in Colin et al. [6] downwards flow experiments. F. Void fraction results in Colin et al. [6] microgravity experiments.

4. BOILING FLOW SIMULATIONS

4.1. The Debora Database

The Debora loop was built at CEA/Grenoble to study boiling flow in reactor conditions by filling similarity criteria [8] (see figure 1). It consists of a vertical Freon-12 pipe with a 1m-long inlet section, a 3.5m-long heated section and an instrumentation plane located 3.485m after the beginning of the heated section. During different campaigns, liquid temperatures, void fractions, gas velocities and Sauter mean diameters were measured.

In the following, we will call a *test tube* a series of runs that have identical outlet pressures, mass flow rates and heating power. Each test tube consists of different runs in which the inlet temperature is varied. Reducing the inlet temperature is equivalent to measuring physical quantities at a lower point in the test section. We call i_{\max} the run of a given test tube at the highest inlet temperature $T_{\text{in},i_{\max}}$. Then the physical quantities measured at the outlet for a run i with an inlet temperature T_i are the same as those measured at an altitude z_i for an inlet temperature $T_{\text{in},i_{\max}}$ such that $X_{T_{\text{in}}=T_i}(z_i) = X_{T_{\text{in}}=T_{\text{in},i_{\max}}}(z_{\text{outlet}})$, with X the thermodynamic quality of the flow. Therefore, in this section we launch calculations for each test tube with

$T_{in} = T_{in,i_{max}}$ et extract the physical parameters at the different z_i . The conditions of the runs that we select are presented in table I.

Test tube	Mass flow rate kg/(m ² s)	Pressure MPa	Heat flux W/m ²	$T_{in,i_{max}}$ °C	z_i m	$X(z_i)$
I	1007	3.01	58.2	73.7	0.72	-0.2165
					1.48	-0.0973
					2.48	0.0585
					2.98	0.1343
					3.485	0.2173
II	2016	1.458	76.26	44.21	0.75	-0.0677
					1.52	-0.0185
					1.81	0.0014
					2.20	0.0261
					2.49	0.046
					2.86	0.0687
3.485	0.1091					
III	2994	2.618	109.3	72.49	1.64	-0.0519
					2.02	-0.0177
					2.41	0.0164
					2.84	0.0479
					3.14	0.077
					3.485	0.1005

Table I. Flow conditions of the Debora cases we study. z_i is taken at the beginning of the heated length. Each z_i matches a run in [8] in which $X_{outlet} = X(z_i)$.

The Sauter mean diameter is measured along the radius of the channel for each z_i . We interpolate the experimental Sauter mean diameter at any (r, z) point in the test section and enforce it in our simulations. We can therefore run simulations without having to predict the mean Sauter diameter in the flow.

4.2. Simulation Configurations and Results

We run the simulations presented in table II. All test tubes are first simulated with our baseline closure laws (simulations 1, 4 and 6). These are the ones used in the adiabatic tube validation, with Kurul&Podowski wall heat transfer [37] and Zeitoun et al. interfacial heat transfer [36]. The baseline simulation results are presented in figure 5-A,D and J.

The Sugrue et al. lift coefficient [17] is void-fraction dependent and goes to 0 from $\alpha = 0.2$ to $\alpha = 0.52$. Therefore, it has no effect on test tube II for $X_i = 0.1091$ (see figure 5-D) and a reduced effect for X_i between 0.046 and 0.1091, which leads to a completely wrong void fraction profile for simulation 4. Furthermore, test tube I is correctly predicted with a Sugrue lift that is close to 0 due to high void fraction (figure 5-A). We confirm the negligible effect of lift on this test tube through a simulation without any lift force (simulation 2, figure 5-B). This means that there are reactor condition flows in which the lift force is essential and others where it doesn't play a key role.

Simulation	Test tube	Lift	Turbulent dispersion	Interfacial heat flux
1	I	Sugrue et al. [17]	Burns et al. [33]	Zeitoun et al. [36]
2	I	No lift	Burns et al. [33]	Zeitoun et al. [36]
3	I	No lift	Burns et al. [33]	Ranz&Marshall [35]
4	II	Sugrue et al. [17]	Burns et al. [33]	Zeitoun et al. [36]
5	II	$C_L = -0.2$	Burns et al. [33]	Zeitoun et al. [36]
6	III	Sugrue et al. [17]	Burns et al. [33]	Zeitoun et al. [36]
7	III	$C_L = -0.2$	$1/2 \cdot$ Burns et al. [33]	Zeitoun et al. [36]

Table II. List of simulation configurations on Debora test tubes presented here. All simulations are carried out with a $k - \omega$ turbulence model [5], Tomiyama et al. drag coefficient [28], Lubchenko et al. wall correction [34] and Kurul&Podowski wall heat flux partition [37].

To obtain a center-peaked void fraction profile in test tube II as in the experiment, we use $C_L = -0.2$ in simulation 5. This value is in-between the deformable bubble lift coefficient from Tomiyama et al. [13], $C_L = -0.28$, and the one from Sugrue [17], $C_L = -0.15$. This greatly improves the simulation results (figure 5-E vs D). As can be seen in the radial force balance, bubbles are first pushed away from the wall by the lift force, before the turbulent dispersion force becomes dominant towards the middle of the channel (figure 5-I). The only significant resisting force is the radial drag force. However, many issues remain: the void fraction is too low at the wall, suggesting the lift force is too strong there; the simulated void fraction for $X_i = 0.0014$ is too low, suggesting insufficient bubble nucleation at the wall or excessive condensation; the void fraction for $X_i = 0.1091$ has a too flat profile, suggesting the lift force is too weak at the core. Enforcing $C_L = -0.2$ for test tube III also makes it possible to obtain a flat profile at the wall (simulation 7, figure 5-L).

We run test tube I with the Ranz&Marshall interfacial heat flux [35] to compare it with the Zeitoun et al. correlation [36] (simulation 3). This improves the void fraction predictions for sub-saturated conditions (figure 5-C vs B). For $X_i = 0.2173$, the flow is saturated and there is no difference between the two.

Test tube II liquid temperature results are surprisingly close to experimental value (figure 5-F) though the void fraction and gas velocity profiles are off. The indicates that single-phase diffusion, and not multiphase effects, is key in the liquid temperature profile.

Axial gas velocities are significantly underestimated, especially at high void fraction (figure 5-G). This means we must improve the drag formulation. Liquid radial velocities are positive and gas negative, indicating they trade places in the tube (figure 5-H). The radial velocity is very void-fraction dependent.

Simulated test tube III void fraction profiles are too high compared with experimental values (figure 5-J,L). Given the amplitude of this discrepancy, it can have four main causes: an underestimated gas flow rate; a liquid superheat; a gas superheat, but this seems more unlikely than for the liquid; a possibly overestimated power measurement on the Debora experiment.

Test tube III relative axial velocities can become negative in the near-wall region (figure 5-K). In the simulation, this is due to slow bubbles moving towards the core and encountering a quicker liquid. To the best of our knowledge, this has not been observed experimentally. This inverts the lift in the near-wall region.

5. CONCLUSIONS

We developed a bubbly-flow CFD framework and selected a set of closure terms that we validated on adiabatic atmospheric-pressure data. Enforcing the experimental diameter in our simulations shows that, independently of interfacial area modeling, this selection of models isn't appropriate for the nuclear reactor-similarity conditions of the Debora experiment. We improved the results by modifying select closure terms.

The next steps in this study will be to obtain a single formulation of interfacial forces and heat transfer closure terms that works for all Debora cases. To simulate accurately reactor-condition flows, we must also predict the local bubble diameter. We have begun work on an interfacial area transport equation approach.

NOMENCLATURE

Subscripts

k	Arbitrary phase
l	Liquid phase phase
g	Gas phase

Greek letters

α_k	Fraction of phase k
Γ_k	Interfacial mass transfer towards phase k
λ_k	Thermal conductivity of phase k
μ_k	Dynamic viscosity of phase k (Pas)
ν_k	Kinetic viscosity of phase k (m^2s^{-1})
ν_t	Turbulent kinetic viscosity of liquid
ρ_k	Volume mass of phase k
Φ	Wall heat flux
ω	Turbulent dissipation frequency of liquid

Dimensionless numbers

$Ja = \frac{\rho_l C_{p,l} \ T_{\text{sat}} - T_l\ }{\rho_g L_{\text{vap}}}$	Jacob number
$Pe = \frac{d_b \ \vec{u}_g - \vec{u}_l\ \cdot \rho C_{p,l}}{\lambda_l}$	Peclet number
$Pr = \frac{\nu_l \cdot \rho C_{p,l}}{\lambda_l}$	liquid Prandtl number
$Re_b = \frac{d_b \ \vec{u}_g - \vec{u}_l\ }{\nu_l}$	bubble Reynolds number

Roman letters

d_b	Bubble diameter
$C_{p,k}$	Heat capacity of phase k
e_k	Internal energy of phase k
\vec{F}_{ki}	Interfacial forces applied to phase k
\vec{g}	Gravity (ms^{-2})
k	Turbulent kinetic energy of liquid
L_{vap}	Evaporation latent heat
q_{ki}	Interfacial heat flux towards phase k
q_{kw}	Wall heat flux towards phase k
$r_+ = \frac{r}{R_{\text{pipe}}}$	Dimensionless radial position
P	Pressure
T_k	Temperature of phase k
T_s	Saturation temperature
T_w	Wall temperature
X	Thermodynamic quality of the flow
y	Distance to wall
$y_+ = \frac{yu_\tau}{\nu_l}$	Dimensionless distance to wall
\vec{u}_k	Velocity of phase k

ACKNOWLEDGMENTS

The authors thank Elie Saikali and Yannick Gorsse for their help in developing TrioCMFD.

REFERENCES

1. D. Lucas et al., "Status and challenges of CFD-modelling for poly-disperde bubbly flow," *Proc. NURETH-16*, (2015).

2. Y. Liao, E. Krepper, and D. Lucas, "A baseline closure concept for simulating bubbly flow with phase change: A mechanistic model for interphase heat transfer coefficient," *Nuclear Engineering and Design*, **348**, pp. 1–13 (2019).
3. A. Gerschenfeld and Y. Gorsse, "Development of a Robust multiphase flow solver on General Meshes; application to sodium boiling at the subchannel scale," *Proc. NURETH 2022*, (2022).
4. P.-E. Angeli, U. Bieder, and G. Fauchet, "Overview of the TrioCFD code: Main features, V&V procedures and typical application to nuclear engineering," *Proc. NURETH-16*, (2015).
5. J. Kok, "Resolving the dependence on free-stream values for the k-omega turbulence model," NLR-TP-99295, National Aerospace Laboratory NLR (1999).
6. C. Colin, J. Fabre, and A. Kamp, "Turbulent bubbly flow in pipe under gravity and microgravity conditions," *Journal of Fluid Mechanics*, **711**, pp. 469–515 (2012).
7. R. Sugrue, B. Magolan, N. Lubchenko, and E. Baglietto, "Assessment of a simplified set of momentum closure relations for low volume fraction regimes in STAR-CCM+ and OpenFOAM," *Annals of Nuclear Energy*, **110**, pp. 79–87 (2017).
8. J. Garnier, E. Manon, and G. Cubizolles, "Local measurements on flow boiling of refrigerant 12 in a vertical tube," *Multiphase Science and Technology* (2001).
9. J.-M. DELHAYE, *Thermohydraulique des réacteurs*, EDP Sciences (2008).
10. N. E. Todreas and M. S. Kazimi, *Nuclear Systems I: Thermal Hydraulic Fundamentals*, CRC press (2021).
11. M. Ishii and T. Hibiki, *Thermo-fluid dynamics of two-phase flow*, Springer Science and Business Media (2006).
12. D. Bestion et al., "Some lessons learned from the use of Two-Phase CFD for Nuclear Reactor Thermalhydraulics," *Proc. The 13th International Topical Meeting on Nuclear Reactor Thermal Hydraulics (NURETH-13)*, (2009).
13. A. Tomiyama, H. Tamai, I. Zun, and S. Hosokawa, "Transverse migration of single bubbles in simple and shear flows," *Chemical Engineering Science*, **57**, pp. 1849–1858 (2002).
14. W. Yao and C. Morel, "Volumetric interfacial area prediction in upward bubbly two-phase flow," *International Journal of Heat and Mass Transfer*, **47** (2), pp. 307–328 (2004).
15. E. Krepper, D. Lucas, T. Frank, H.-M. Prasser, and P. J. Zwart, "The inhomogeneous MUSIG model for the simulation of polydispersed flows," *Nuclear Engineering and Design*, **238** (7), pp. 1690–1702 (2008).
16. C. Yuan, F. Laurent, and R. Fox, "An extended quadrature method of moments for population balance equations," *Journal of Aerosol Science*, **51**, pp. 1–23 (2012).
17. R. Sugrue, *A Robust Momentum Closure Approach for Multiphase Computational Fluid Dynamics Applications*, PhD thesis, 2017.
18. T.-J. Chuang and T. Hibiki, "Interfacial forces used in two-phase flow numerical simulation," *International Journal of Heat and Mass Transfer*, **113**, pp. 741–754 (2017).
19. T. Hibiki, M. Ishii, and Z. Xiao, "Axial interfacial area transport of vertical bubbly flows," *International Journal of Heat and Mass Transfer*, **44**, pp. 1869–1888 (2001).
20. I. Park, H. Cho, H. Yoon, and J. Jeong, "Numerical effects of the semi-conservative form of momentum equations for multi-dimensional two-phase flows," *Nuclear Engineering and Design*, **239**, pp. 2365–2371 (2009).

21. T. Franck, S. Jain, A. Matyushenko, and A. Garbaruk, "The OECD/NEA MATHIS-H benchmark - CFD analysis of water flow through a 5x5 rod bundle with spacer grids using Ansys Fluent and Ansys CFX," *Proc. CFD4NRS-4, Conference on Experimental Validation and Application of CFD and CMFD Codes in Nuclear Reactor Technology, OECD/NEA and IAEA Workshop*, (2012).
22. F. R. Menter, "Zonal Two Equation k- ϵ Turbulence Models for Aerodynamic Flows," *Proc. American Institute of Aeronautics and Astronautics 24th Fluid Dynamics Conference*, (1993), American Institute of Aeronautics and Astronautics, AIAA 93-2906.
23. J.-R. Carlson, V. N. Vatsay, and J. Whitey, "Node-Centered Wall Function Models for the Unstructured Flow Code Fun3D," *Proc. 22nd AIAA Computational Fluid Dynamics Conference*, pp. 2758 (2015).
24. T. Knopp, T. Alrutz, and D. Schwamborn, "A grid and flow adaptive wall-function method for RANS turbulence modelling," *Journal of Computational Physics*, **220**, pp. 19–40 (2006).
25. B. Kader, "Temperature and concentration profiles in fully turbulent boundary layers," *Int. J. Heat Mass Transfer*, **24** (9), pp. 1541–1544 (1981).
26. E. Almeras, V. Mathai, D. Lohse, and C. Sun, "Experimental investigation of the turbulence induced by a bubble swarm rising within incident turbulence," *J. Fluid Mech.*, **825**, pp. 1091–1112 (2017).
27. H. Reichardt, "Vollständige Darstellung der turbulenten Geschwindigkeitsverteilung in glatten Leitungen," *Z. angew. Math. Mech.*, **31** (7), pp. 208–219 (1951).
28. A. Tomiyama, I. Kataoka, I. Zun, and T. Sakaguchi, "Drag Coefficients of Single Bubbles under Normal and Micro Gravity Conditions," *JSME International Journal Series B Fluids and Thermal Engineering* (1998).
29. D. Drew and R. Lahey, "The virtual mass and lift force on a sphere in rotating and straining inviscid flow," *Int. J. Multiphase Flow*, **13** (1), pp. 113–121 (1987).
30. N. Zuber, "On the dispersed two-phase flow in the laminar flow regime," *Chemical Engineering Science*, **19**, pp. 897–917 (1964).
31. C. Béguin, . Pelletier, and S. Étienne, "Void fraction influence on added mass in a bubbly flow," *European Journal of Mechanics B/Fluids*, **56**, pp. 28–45 (2016).
32. C. Garnier, M. Lance, and J. Marie, "Measurement of local flow characteristics in buoyancy-driven bubbly flow at high void fraction," *Experimental Thermal and Fluid Science*, **26**, pp. 811–815 (2002).
33. A. D. Burns, T. Frank, I. Hamill, , and J.-M. Shi, "The Favre Averaged Drag Model for Turbulent Dispersion in Eulerian Multi-Phase Flows," *Proc. 5th International Conference on Multiphase Flow*, (2004).
34. N. Lubchenko, B. Magolan, R. Sugrue, and E. Baglietto, "A more fundamental wall lubrication force from turbulent dispersion regularization for multiphase CFD applications," *International Journal of Multiphase Flow*, **98**, pp. 36–44 (2018).
35. W. E. Ranz and W. Marshall, "Evaporation from droplets," *Chem. Eng. Prog.*, **48** (3), pp. 141–146 (1952).
36. O. Zeitoun, M. Shoukri, and V. Chatoorgoon, "Interfacial Heat Transfer Between Steam Bubbles and Subcooled Water in Vertical Upward Flow," *Proc. Transactions of the ASME*, (1995).
37. N. Kurul and M. Podowski, *Proc. International Heat Transfer Conference Digital Library*, (1990).
38. V. Bergeaud and V. Lefebvre, "SALOME. A software integration platform for multi-physics, pre-processing and visualisation.," *Proc. Proceedings of SNA + MC2010: Joint international conference on supercomputing in nuclear applications + Monte Carlo Tokyo*, (2010).

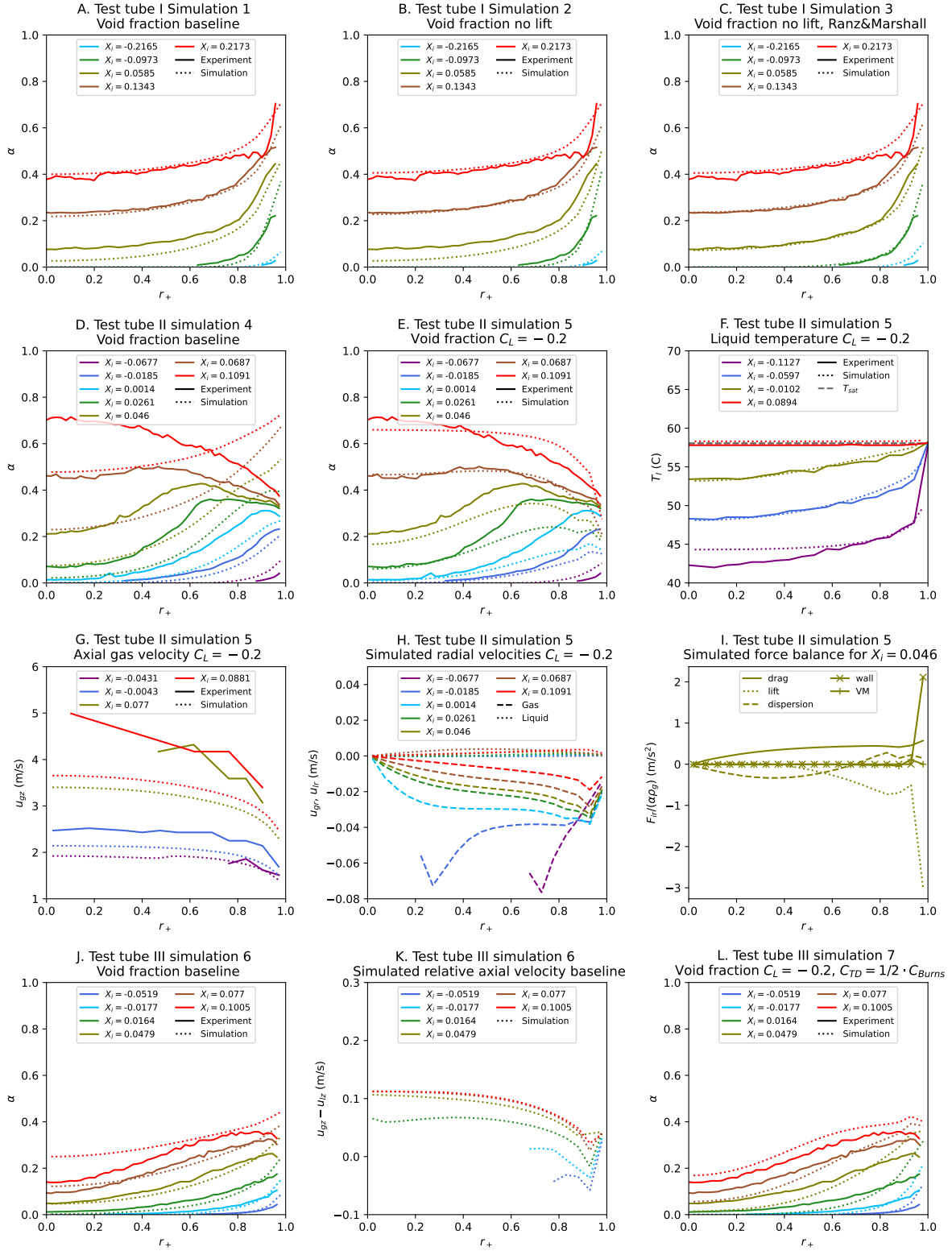


Figure 5. Results of our simulations on the Debora setup. The simulation configurations can be found in table II. A-C. Test tube I results. D-I. Test tube II results. J-L. Test tube III results. A-E. Simulation 1-5 void fraction results. F-G. Simulation 5-6 liquid temperature and axial gas velocity results. H-I. Physical quantities extracted from simulation 5: radial velocities and force balance for $X_i = 0.046$. J&L. Simulation 6&7 void fraction results. K. Simulation 6 relative velocity profiles.